Science Advances
AAAS

advances.sciencemag.org/cgi/content/full/6/29/eabc0810/DC1

Supplementary Materials for

De novo rational design of a freestanding, supercharged polypeptide, proton-conducting membrane

Chao Ma, Jingjin Dong, Marco Viviani, Isotta Tulini, Nicola Pontillo, Sourav Maity, Yu Zhou, Wouter H. Roos, Kai Liu*, Andreas Herrmann*, Giuseppe Portale*

*Corresponding author. Email: kai.liu@ciac.ac.cn (K.L.); herrmann@dwi.rwth-aachen.de (A.H.); g.portale@rug.nl (G.P.)

Published 17 July 2020, *Sci. Adv.* **6**, eabc0810 (2020)
DOI: 10.1126/sciadv.abc0810

This PDF file includes:

Figs. S1 to S8
Tables S1 and S2
References

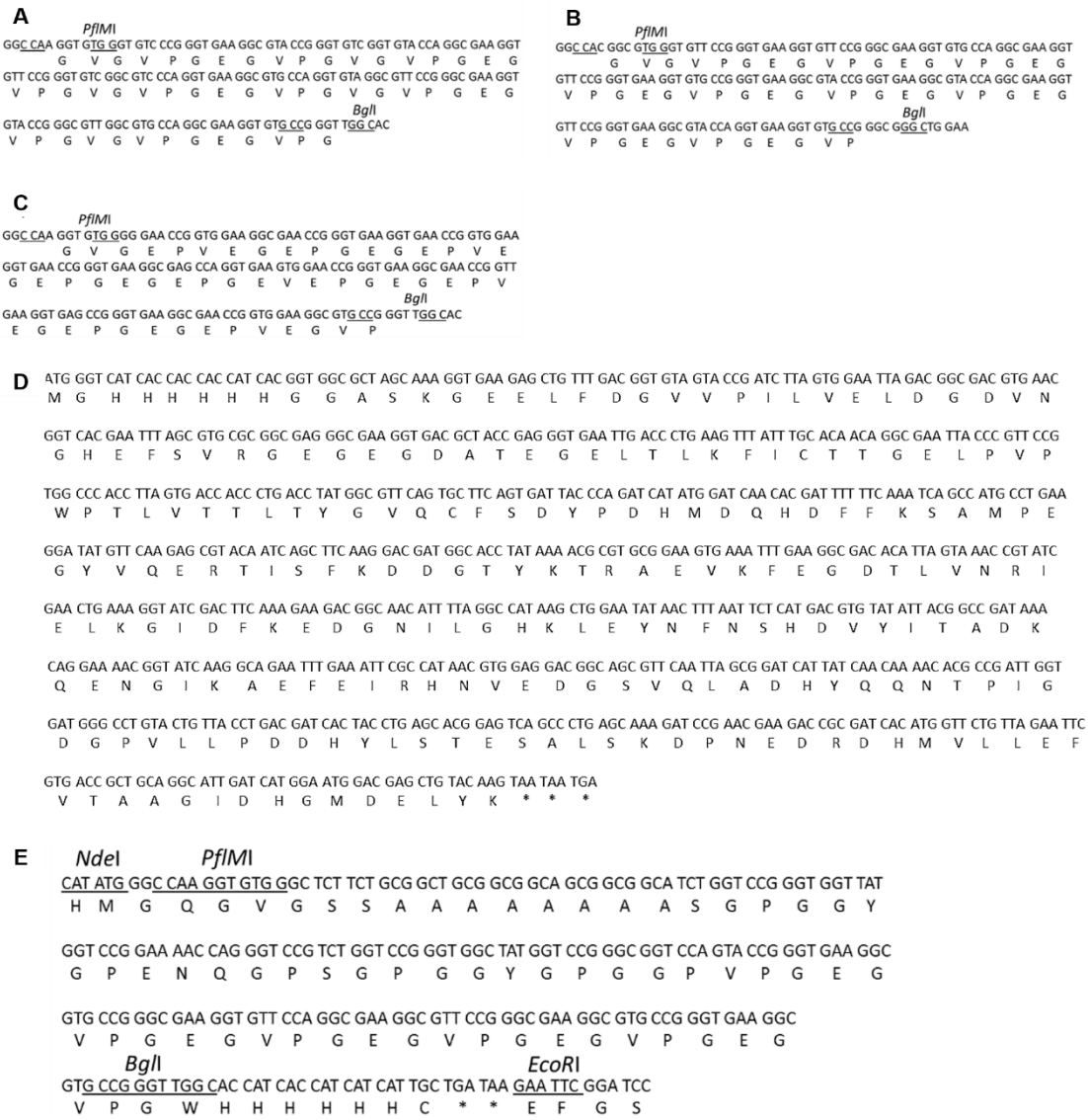

Figure S1. Gene fragments and corresponding polypeptide sequences of monomeric SUP sequences. (A) Half charged monomer, HC_E5, containing 5 glutamic acids, (B) Single charged monomer, E9, containing 9 glutamic acids and (C) double charged monomer, DC_E18, containing 18 glutamic acid residues. Restriction sites flanking the inserted genes are *PflM*I and *Bgl*I with the help of which gene oligomerization was performed. (D) Gene fragment and amino acid sequence of -30 GFP used in this study. (E) Gene fragment and corresponding polypeptide sequence of monomeric spider-E chimera. The full length of amino acid sequence of spider-E is listed in Table S1.

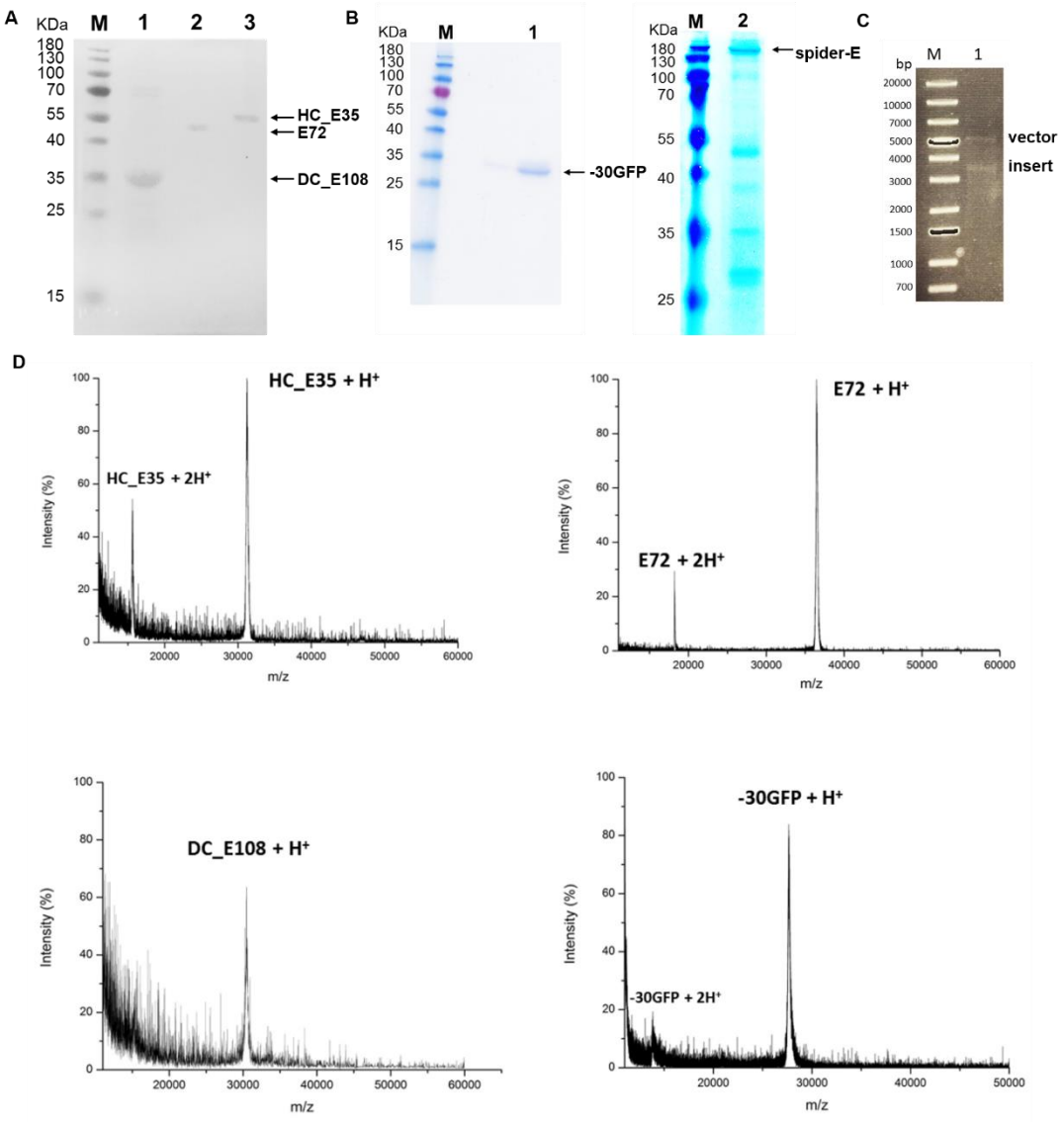

Figure S2. Protein characterizations with PAGE and MALDI-TOF. (A) SDS-PAGE characterization of unstructured SUP samples used in this study. Lane 1, DC_E108; Lane 2, E72; Lane 3, HC_E35. The electrophoretic behavior of the SUPs with different net charge densities varies, although they exhibit similar molecular weights as shown in Table S1. (B) SDS-PAGE characterization of folded and β-sheet containing protein samples used in this study. Lane 1, -30GFP; Lane 2, spider-E. The electrophoretic behavior of the supercharged proteins with high net charges is different from other proteins, which usually exhibit balanced charges on the surface compare ladder proteins shown in lane M). The low electrophoretic mobility of spider-E is probably due to strong hydrogen bonding and formation of larger aggregates. (C) The restriction enzyme digest of the constructed plasmid pET spider-E with *Nde*I and

*EcoR*I is shown. In lane 1, the upper band shows digested vector backbone, ca. 5300 bp, and the lower band (ca. 3500 bp) is the inserted gene accommodating eighteen repeats of monomeric spider-E. M, standard DNA ladder. (D) MALDI-TOF mass spectra of supercharged polypeptides and proteins used in this study. It is worth noting that the Mw of spider-E sample is too large to be determined using MALDI TOF mass spectrometry with which typically molecular ion peaks of less than 50 KDa are determined. Thus, biophysical measurements, like FTIR and GIXD (Fig. 3 and Fig. S8), were applied for the characterization of the spider-E sample.

Table S1. General information of the samples used in this study, including isoelectric point, molecular formula, molecular weight, charge density and expression yield.

SUPs	Isoelectric point	Formula	Mw(Da)	Charge Density $(N_{posAA}-N_{negAA})/N_{AA}$	Expression Yield (mg/L)
HC_E35	3.79	GQ $[(GVGVPGEGVP)_5]_7GWH_6C$	31217	-0.09	30-50
E72	3.45	$GAGP[(GVGVP)(GEGVP)_9]_8GWPH_6$	36512	-0.18	30-50
DC_E108	3.27	GQ[GVGEPVEGEPGEGEPVEGEPGEGEPGEVEPGEGEPVE GEPGEGEPVEGVP]$_6$GWH_6C	30442	-0.35	30-50
-30 GFP	4.64	Shown in Figure S2	27789	-0.12	~30
Spider-E	3.32	MGQ(GVGSSAAAAAAAASGPGGYGPENQGPSGPGGYGPGGPVP GEGVPGEGVPGEGVPGEGVPGEGVP)$_{18}$GWH_6C	99412	-0.1	~10

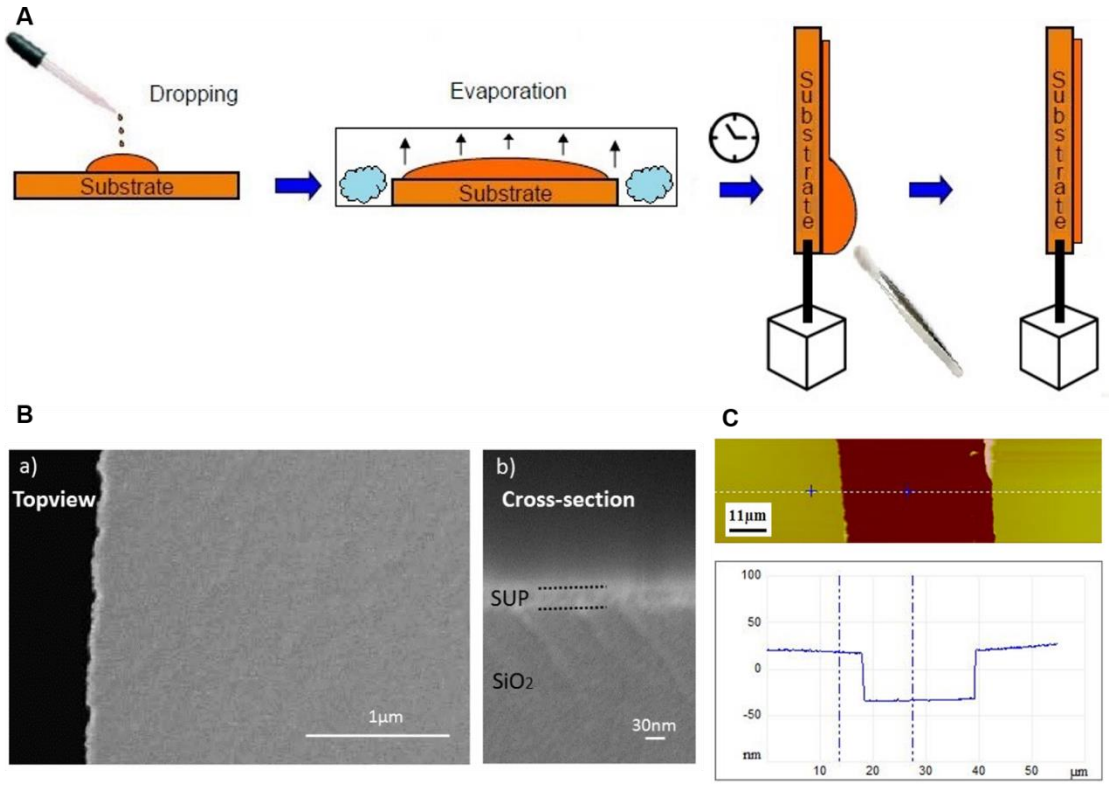

Figure S3. Protein films on substrates and characterization via SEM and AFM. (A) Schematic procedure for the preparation of proton conducting polypeptide and protein films by the drop casting technique used in this study. (B) Scanning electron microscopy (SEM) images showing the flat and homogenous morphology of our customized thin film (here E72 is shown as an example) on the electrodes. The jagged edge on the left side of a) is the truncating position for cross-section imaging in b). (C) AFM image of a scratched thin film surface (top) and its corresponding height profile (bottom). E72 is shown here as an example.

Table S2. All the protein samples on the IDE electrodes exhibit an average height of ca. 30-50 nm as determined by AFM. Each data set consists of three different films measured individually at various positions.

Sample	Thickness (nm)			Average Thickness (nm)
HC-35	44±2	48±1	48±2	47±2
E72	47±3	34±3	39±6	40±5
DC-108	33±2	31±5	44±3	36±6
-30GFP	29±3	27±4	30±2	29±1
spider-E	43±3	40±4	49±2	44±4

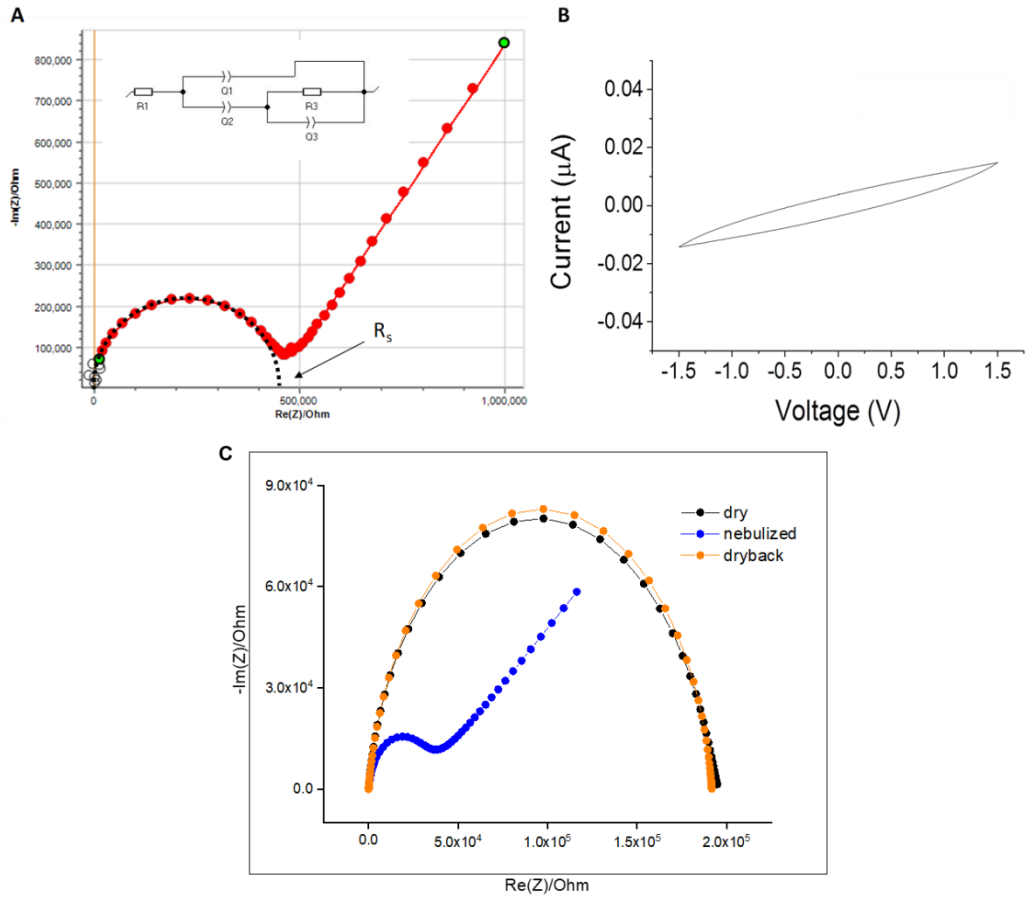

Figure S4. **Nyquist plots of protein film devices**. (A) Typical Nyquist plot of a protein film. Red circles are the experimental data and the red line is the fit using the equivalent circuit reported in the inset. The first semicircle whose intercept with the x axis provides the sample resistance is also highlighted for clarity. (B) Typical electrical response of humidified spider-E film. Current versus voltage measurements of a spider-E FS film taken at RH = 90%. (C) Nebulization test curves in EIS to evaluate the stability of the cast thin film on IDE electrode upon direct exposure to water.

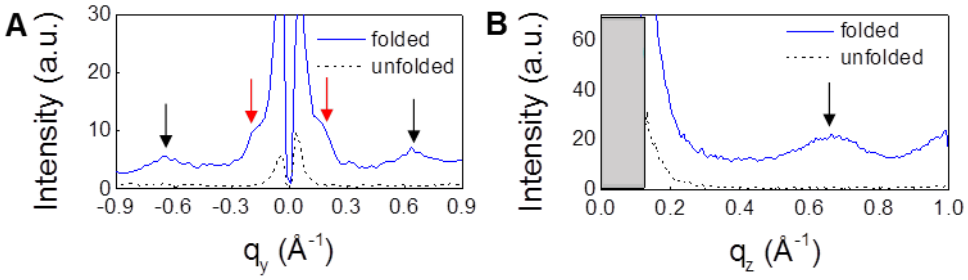

Figure S5. **X-Ray characterization of E72 and -30GFP protein films on the electrodes**. (A) Horizontal and (B) vertical GIXD intensity cuts of the folded (-30GFP, blue solid line) and the unfolded (E72, black dashed line) protein films. The black and the red arrows in (A) and (B) highlight the position of the two symmetric diffraction peaks for the -30GFP protein film located at $q \approx 0.65$ Å^{-1} and $q \approx 0.18$ Å^{-1}, respectively.

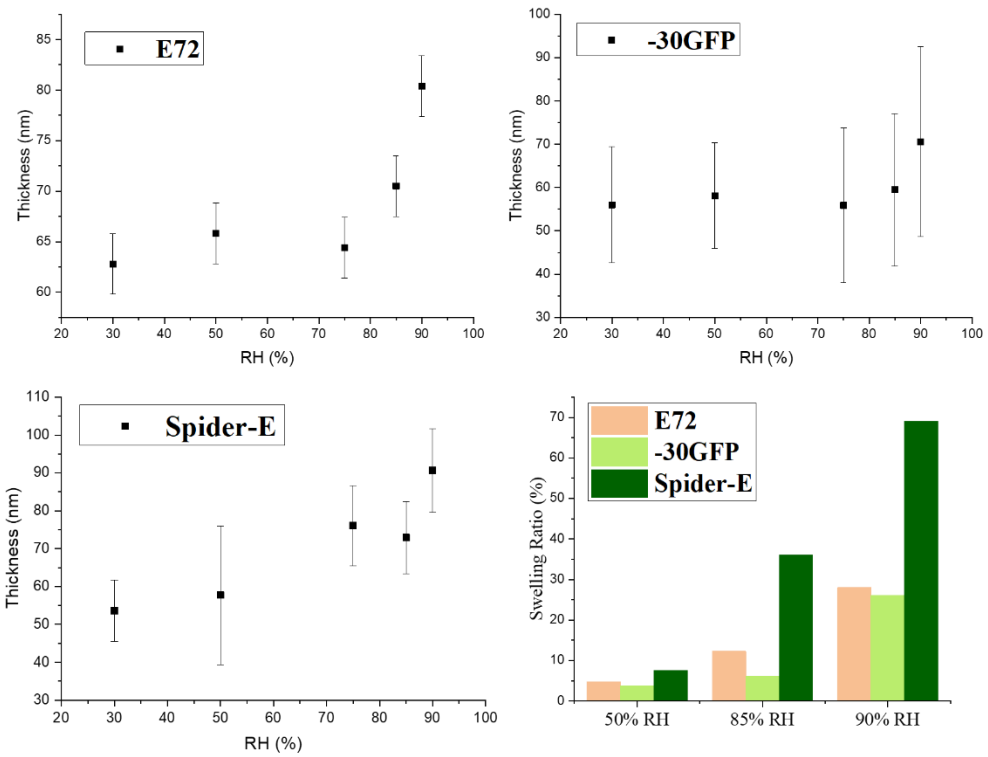

Figure S6. The thickness and swelling ratio of the protein films on electrodes at different RHs.

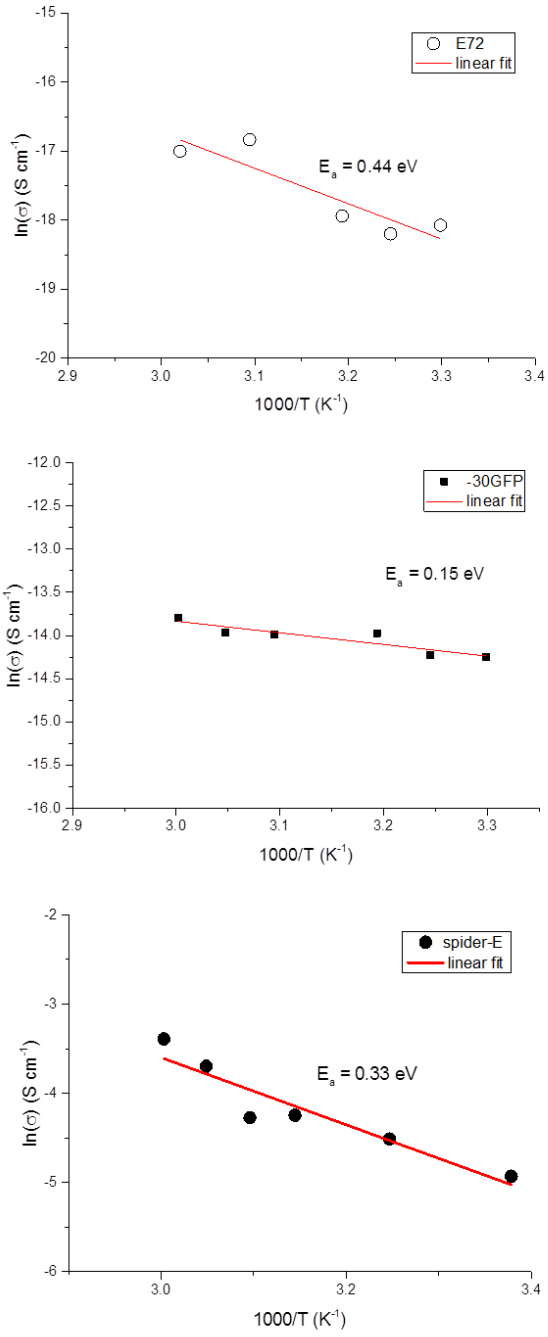

Figure S7. **Temperature dependent proton conductivity measurements** performed at RH = 90% from 298K over 330K in order to estimate the activation energy for the protein-based systems. The activation energy was estimated from the values of the slopes in the linearized Arrhenius plots. Thin films prepared from E72, -30GFP, spider-E samples were employed for the tests.

A

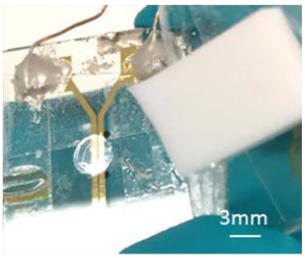

C

Materials	type	Elastic Modulus (GPa)	Yield Strength (MPa)	Strain (%)	Reference
Natural spider silk	Fiber	4	800-1100	35	*(46)*
Recombinant spider silk	Film	0.3	54	2	*(47)*
spider-E	Film	0.22	38	500	This work
Collagen	Film	0.05	8	100	*(48)*
Collagen X-linked	Film	1	47	20	*(48)*

B

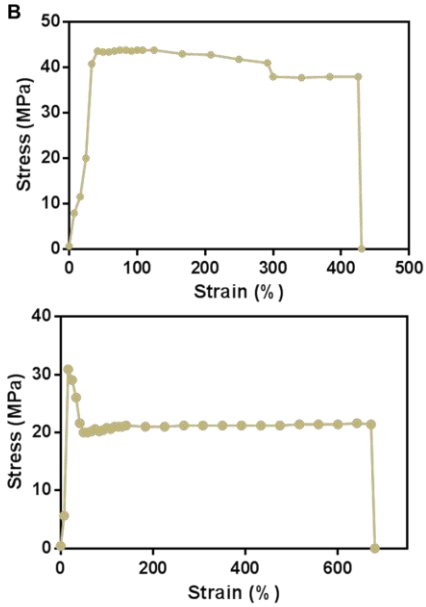

D

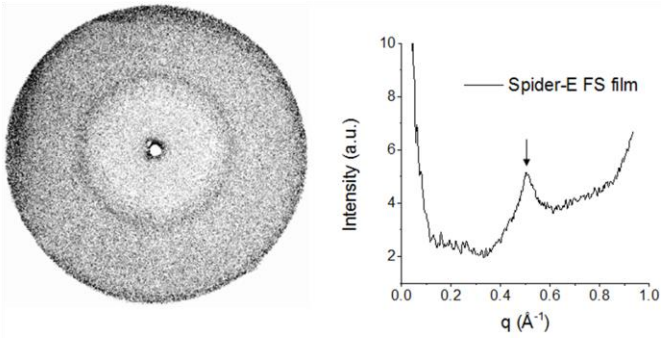

Figure S8. **Freestanding spider-E protein device assembly, mechanical and structural characterization**. (A) The prepared spider-E membrane assembled on a Y-shape electrode for the EIS data collection. Photo credit: Chao Ma, University of Groningen. (B) The mechanical characterizations of spider-E membranes through tensile-stress device. (C) Data compiling of engineered protein films. (D) Structural characterization of chimeric spider-E freestanding (FS) film using transmission small angle X-ray scattering (SAXS). A typical inter-sheet distance of 12 Å between stacked beta-sheets is revealed. The black arrow indicates the respective diffraction peak (q = 0.52 $Å^{-1}$, d = 12 Å).

REFERENCES AND NOTES

1. N. A. Kotov, J. O. Winter, I. P. Clements, E. Jan, B. P. Timko, S. Campidelli, S. Pathak, A. Mazzatenta, C. M. Lieber, M. Prato, R. V. Bellamkonda, G. A. Silva, N. W. S. Kam, F. Patolsky, L. Ballerini, Nanomaterials for neural interfaces. *Adv. Mater.* **21**, 3970–4004 (2009).

2. M. Valiadi, D. Iglesias-Rodriguez, Understanding bioluminescence in dinoflagellates—How far have we come? *Microorganisms* **1**, 3–25 (2013).

3. I. N. Watt, M. G. Montgomery, M. J. Runswick, A. G. Leslie, J. E. Walker, Bioenergetic cost of making an adenosine triphosphate molecule in animal mitochondria. *Proc. Natl. Acad. Sci. U.S.A.* **107**, 16823–16827 (2010).

4. Y. Sudo, A. Okazaki, H. Ono, J. Yagasaki, S. Sugo, M. Kamiya, L. Reissig, K. Inoue, K. Ihara, H. Kandori, S. Takagi, S. Hayashi, A blue-shifted light-driven proton pump for neural silencing. *J. Biol. Chem.* **288**, 20624–20632 (2013).

5. E. B. Trigg, T. W. Gaines, M. Maréchal, D. E. Moed, P. Rannou, K. B. Wagener, M. J. Stevens, K. I. Winey, Self-assembled highly ordered acid layers in precisely sulfonated polyethylene produce efficient proton transport. *Nat. Mater.* **17**, 725–731 (2018).

6. K.-D. Kreuer, G. Portale, A critical revision of the nano-morphology of proton conducting ionomers and polyelectrolytes for fuel cell applications. *Adv. Funct. Mater.* **23**, 5390–5397 (2013).

7. J. Molina, J. J. de Pablo, J. P. Hernández-Ortiz, Structure and proton conduction in sulfonated poly(ether ether ketone) semi-permeable membranes: A multi-scale computational approach. *Phys. Chem. Chem. Phys.* **21**, 9362–9375 (2019).

8. S. S. Nagarkar, S. M. Unni, A. Sharma, S. Kurungot, S. K. Ghosh, Two-in-one: Inherent anhydrous and water-assisted high proton conduction in a 3D metal-organic framework. *Angew. Chem.* **126**, 2676–2680 (2014).

9. M. R. Karim, K. Hatakeyama, T. Matsui, H. Takehira, T. Taniguchi, M. Koinuma, Y. Matsumoto, T. Akutagawa, T. Nakamura, S.-i. Noro, T. Yamada, H. Kitagawa, S. Hayami, Graphene oxide nanosheet with high proton conductivity. *J. Am. Chem. Soc.* **135**, 8097–8100 (2013).

10. J. A. Hurd, R. Vaidhyanathan, V. Thangadurai, C. I. Ratcliffe, I. L. Moudrakovski, G. K. H. Shimizu, Anhydrous proton conduction at 150 °C in a crystalline metal–organic framework. *Nat. Chem.* **1**, 705–710 (2009).

11. R. Fan, S. Huh, R. Yan, J. Arnold, P. Yang, Gated proton transport in aligned mesoporous silica films. *Nat. Mater.* **7**, 303–307 (2008).

12. C. Zhong, Y. Deng, A. F. Roudsari, A. Kapetanovic, M. P. Anantram, M. Rolandi, A polysaccharide bioprotonic field-effect transistor. *Nat. Commun.* **2**, 476 (2011).

13. D. D. Ordinario, L. Phan, W. G. Walkup IV, J.-M. Jocson, E. Karshalev, N. Hüsken, A. A. Gorodetsky, Bulk protonic conductivity in a cephalopod structural protein. *Nat. Chem.* **6**, 596–602 (2014).

14. N. Amdursky, X. Wang, P. Meredith, D. D. C. Bradley, M. M. Stevens, Long-range proton conduction across free-standing serum albumin mats. *Adv. Mater.* **28**, 2692–2698 (2016).

15. Y. Guo, Z. Jiang, W. Ying, L. Chen, Y. Liu, X. Wang, Z.-J. Jiang, B. Chen, X. Peng, A DNA-threaded ZIF-8 membrane with high proton conductivity and low methanol permeability. *Adv. Mater.* **30**, 1705155 (2017).

16. A. Pena-Francesch, H. Jung, M. A. Hickner, M. Tyagi, B. D. Allen, M. C. Demirel, Programmable proton conduction in stretchable and self-healing proteins. *Chem. Mater.* **30**, 898–905 (2018).

17. X. Strakosas, J. Selberg, Z. Hemmatian, M. Rolandi, Taking electrons out of bioelectronics: From bioprotonic transistors to ion channels. *Adv. Sci.* **4**, 1600527 (2017).

18. X. Liu, H. Gao, J. E. Ward, X. Liu, B. Yin, T. Fu, J. Chen, D. R. Lovley, J. Yao, Power generation from ambient humidity using protein nanowires. *Nature* **578**, 550–554 (2020).

19. N. Agmon, The Grotthuss mechanism. *Chem. Phys. Lett.* **244**, 456–462 (1995).

20. K. L. Naughton, L. Phan, E. M. Leung, R. Kautz, Q. Lin, Y. Van Dyke, B. Marmiroli, B. Sartori, A. Arvai, S. Li, M. E. Pique, M. Naeim, J. P. Kerr, M. J. Aquino, V. A. Roberts, E. D. Getzoff, C. Zhu, S. Bernstorff, A. A. Gorodetsky, Self-assembly of the cephalopod protein reflectin. *Adv. Mater.* **28**, 8405–8412 (2016).

21. J. Lerner Yardeni, M. Amit, G. Ashkenasy, N. Ashkenasy, Sequence dependent proton conduction in self-assembled peptide nanostructures. *Nanoscale* **8**, 2358–2366 (2016).

22. O. Kim, K. Kim, U. H. Choi, M. J. Park, Tuning anhydrous proton conduction in single-ion polymers by crystalline ion channels. *Nat. Commun.* **9**, 5029 (2018).

23. P. Ramaswamy, R. Matsuda, W. Kosaka, G. Akiyama, H. J. Jeon, S. Kitagawa, Highly proton conductive nanoporous coordination polymers with sulfonic acid groups on the pore surface. *Chem. Commun.* **50**, 1144–1146 (2014).

24. A. Pena-Francesch, M. C. Demirel, Squid-inspired tandem repeat proteins: Functional fibers and films. *Front. Chem.* **7**, 69 (2019).

25. S. Studer, D. A. Hansen, Z. L. Pianowski, P. R. E. Mittl, A. Debon, S. L. Guffy, B. S. Der, B. Kuhlman, D. Hilvert, Evolution of a highly active and enantiospecific metalloenzyme from short peptides. *Science* **362**, 1285 (2018).

26. C. Zeymer, D. Hilvert, Directed evolution of protein catalysts. *Annu. Rev. Biochem.* **87**, 131–157 (2018).

27. J. R. Simon, N. J. Carroll, M. Rubinstein, A. Chilkoti, G. P. López, Programming molecular self-assembly of intrinsically disordered proteins containing sequences of low complexity. *Nat. Chem.* **9**, 509–515 (2017).

28. C. Ma, A. Malessa, A. J. Boersma, K. Liu, A. Herrmann, Supercharged proteins and polypeptides. *Adv. Mater.* 1905309 (2020).

29. C. Ma, J. Su, B. Li, A. Herrmann, H. Zhang, K. Liu, Solvent-free plasticity and programmable mechanical behaviors of engineered proteins. *Adv. Mater.* **32**, e1907697 (2020).

30. Y. Daiko, K. Katagiri, A. Matsuda, Proton conduction in thickness-controlled ultrathin polycation/nafion multilayers prepared via layer-by-layer assembly. *Chem. Mater.* **20**, 6405–6409 (2008).

31. C. Yin, J. Li, Y. Zhou, H. Zhang, P. Fang, C. He, Phase separation and development of proton transport pathways in metal oxide nanoparticle/nafion composite membranes during water uptake. *J. Phys. Chem. C* **122**, 9710–9717 (2018).

32. A. Onuma, J. Kawaji, M. Morishima, T. Mizukami, Y. Takamori, K. Yamaga, Effects of micro-phase-separated structures on proton conductivity and methanol permeability in polymer electrolyte membranes. *Polymer* **55**, 2673–2677 (2014).

33. M. S. Lawrence, K. J. Phillips, D. R. Liu, Supercharging proteins can impart unusual resilience. *J. Am. Chem. Soc.* **129**, 10110–10112 (2007).

34. J. Dou, A. A. Vorobieva, W. Sheffler, L. A. Doyle, H. Park, M. J. Bick, B. Mao, G. W. Foight, M. Y. Lee, L. A. Gagnon, L. Carter, B. Sankaran, S. Ovchinnikov, E. Marcos, P.-S. Huang, J. C. Vaughan, B. L. Stoddard, D. Baker, De novo design of a fluorescence-activating β-barrel. *Nature* **561**, 485–491 (2018).

35. F. Rico, A. Rigato, L. Picas, S. Scheuring, Mechanics of proteins with a focus on atomic force microscopy. *J. Nanobiotechnology* **11** Suppl 1, S3 (2013).

36. E. L. Morley, D. Robert, Electric fields elicit ballooning in spiders. *Curr. Biol.* **28**, 2324–2330.e2 (2018).

37. Q. Wang, H. C. Schniepp, Strength of recluse spider's silk originates from nanofibrils. *ACS Macro Lett.* **7**, 1364–1370 (2018).

38. S. J. Roeters, A. Iyer, G. Pletikapić, V. Kogan, V. Subramaniam, S. Woutersen, Evidence for intramolecular antiparallel beta-sheet structure in alpha-synuclein fibrils from a combination of two-dimensional infrared spectroscopy and atomic force microscopy. *Sci. Rep.* **7**, 41051 (2017).

39. M. C. Piontek, W. H. Roos, Atomic force microscopy: An introduction, in *Single Molecule Analysis: Methods and Protocols,* E. J. G. Peterman, Ed. (Springer, 2018), pp. 243–258.

40. C. A. Wraight, Chance and design—Proton transfer in water, channels and bioenergetic proteins. *Biochim. Biophys. Acta* **1757**, 886–912 (2006).

41. S. Cukierman, Et tu, Grotthuss! and other unfinished stories. *Biochim. Biophys. Acta* **1757**, 876–885 (2006).

42. N. A. Oktaviani, A. Matsugami, A. D. Malay, F. Hayashi, D. L. Kaplan, K. Numata, Conformation and dynamics of soluble repetitive domain elucidates the initial β-sheet formation of spider silk. *Nat. Commun.* **9**, 2121 (2018).

43. Y. Wang, P. Katyal, J. K. Montclare, Protein-engineered functional materials. *Adv. Healthc. Mater.* **8**, e1801374 (2019).

44. X. Hu, P. Cebe, A. S. Weiss, F. Omenetto, D. L. Kaplan, Protein-based composite materials. *Mater. Today* **15**, 208–215 (2012).

45. N. A. Carter, T. Z. Grove, Functional protein materials: Beyond elastomeric and structural proteins. *Polym. Chem.* **10**, 2952–2959 (2019).

46. R. V. Lewis, Spider silk: Ancient ideas for new biomaterials. *Chem. Rev.* **106**, 3762–3774 (2006).

47. J. G. Hardy, A. Leal-Egaña, T. R. Scheibel, Engineered spider silk protein-based composites for drug delivery. *Macromol. Biosci.* **13**, 1431–1437 (2013).

48. C. L. Tucker, J. A. Jones, H. N. Bringhurst, C. G. Copeland, J. B. Addison, W. S. Weber, Q. Mou, J. L. Yarger, R. V. Lewis, Mechanical and physical properties of recombinant spider silk films using organic and aqueous solvents. *Biomacromolecules* **15**, 3158–3170 (2014).